DOI: 10.13009/EUCASS2023-407
Aerospace Europe Conference 2023 – 10TH EUCASS – 9TH CEAS

Dynamic Instability of a Thin-Shell Type Aeroshell Capsule with Pitching Motion in Transonic wind Tunnel

Hideto TAKASAWA[*1], Tomoya Fujii[2], Koshiro Hirata[3], Takahiro Moriyoshi[4], Yusuke Takahashi[1], Yasunori Nagata[5], Kazuhiko Yamada[5]*

[1] *Hokkaido University, 060-8628, Hokkaido, Japan*
[2] *Waseda University, 169-8555, Tokyo, Japan*
[3] *Tokyo University of Agriculture and Technology, 183-8538, Tokyo, Japan*
[4] *Kanazawa Institute of Technology, 924-0838, Kanazawa, Japan*
[5] *Institute of Space and Astronautical Science, Japan Aerospace Exploration Agency, 252-5210, Kanagawa, Japan*

thide3224@eis.hokudai.ac.jp – tomoya747380ny@gmail.com – hira180611@st.go.tuat.ac.jp – moriyoshi@neptune.kanazawa-it.ac.jp – ytakahashi@eng.hokudai.ac.jp – nagata.yasunori@jaxa.jp – yamada.kazuhiko@jaxa.jp
* Corresponding author

Abstract
A mitigation scheme for instability in attitude for deep space sample return capsule is highly demanded. A one-axis free oscillation test in a transonic wind tunnel (TWT) was conducted to construct the method to mitigate instability. For the test, models with varying moment of inertia and inflated rear surfaces were used. It was observed that increasing the moment of inertia in the reference shape resulted in a larger amplitude of angle of attack (AOA). However, by inflating the rear surface, it was possible to reduce the mean amplitude of AOA even with the similar moment of inertia.

1. Introduction

Stable flight in all velocity region is required to the sample return capsule, which reentry into Earth's atmosphere, to realize a safe return to Earth. Thus, the appropriate aerodynamic shape to mitigate aerodynamic instability have to be designed. Previously, Hayabusa2 successfully achieved sample return from an asteroid. Currently, sample return from deeper space is desired. Supposing a sample return mission from the Saturnian region, the reentry velocity into Earth's atmosphere would reach up to 15 km/s, subjecting the capsule to intense aerodynamic heating. To mitigate this aerodynamic heating, a deep-space sample return capsule (DS-SRC) [1] with a lightweight and large-area aeroshell has been proposed, as shown in Figure 1. This capsule, with its low ballistic coefficient, is designed to decelerate from higher altitudes with lower atmospheric density, thereby suppressing aerodynamic heating. Additionally, the capsule is expected to achieve sufficient aerodynamic deceleration, enabling a parachute-less landing.

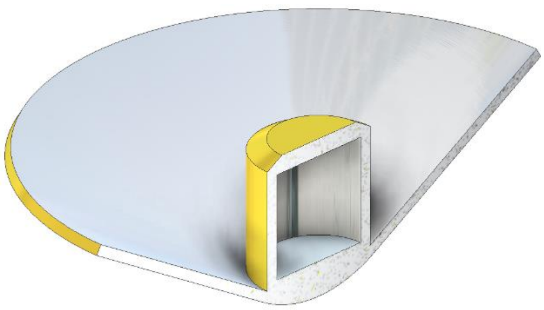

Figure 1: Images of thin-shell type capsule

DOI: 10.13009/EUCASS2023-407

It is desirable for the capsule to maintain proper attitude throughout its flight, ensuring that it does not exhibit rotational divergence in attitude motion at any speed range, including the low-speed regime just before landing. However, studies on instability are still insufficient, and even in the case of the Hayabusa2 capsule [2], a phenomenon of gradually increasing oscillation has been observed. If the capsule becomes unstable in attitude, the landing speed can become too high, and there is a risk that it cannot absorb the impact properly due to incorrect orientation. To increase the success rate of sample return missions, methods to suppress this instability need to be developed. Regarding the static stability of this capsule, wind tunnel tests and numerical analysis [3] have suggested stability across the entire speed range up to Mach 4. Furthermore, in the low-speed regime below Mach 0.3, stability has been indicated through free-flight tests from an altitude of 25 km using a balloon [4].

Parameters affecting aerodynamic instability have been confirmed that factors such as the center of gravity, length of the rear, and roundness of the front. Causes that induce instability are separation [5] or phase delay of pressure [6]. Although several studies are conducted, no methods have been proposed to mitigate aerodynamic instability across the entire range of velocities.

Therefore, in this study, we evaluate the stability of the thin-shell aeroshell-type capsule in the transonic regime and construct methods to reduce instability. We assess instability through pitch-direction one-axis free oscillation tests using Institute of Space and Astronautical Science (ISAS) transonic wind tunnel transonic wind tunnel. Compared to other testing methods such as forced oscillation testing, this testing method [7] has the advantage of simpler testing equipment. As the phase delay of pressure in the wake affect instability, we modify the capsule shape. However, to estimate the impact on other parameters resulting from these modifications, we also conduct evaluations of the influence of the moment of inertia.

2. Wind tunnel test

The wind tunnel tests were conducted using an ISAS transonic wind tunnel at the Japan Aerospace Exploration Agency (JAXA) to evaluate instability of the thin aeroshell capsule. The TWT were the blow-down-type facilities. Both test section sizes had a 0.6 × 0.6 m square cross-section.

In this experiment, the behavior of the capsule in the pitch direction was obtained. The measured items were time history of angle of attack (pitch angle) and pressure in wake region, and flow field using Schlieren visualization. The measurement equipment used is listed in Table 1. A rotating position sensor was used to obtain the AOA. For pressure measurement, a flush-mounted type sensor was selected.

Table 1: Measurement equipment

Position sensor	RDC501051A (ALPS ALPINE CO., LTD.)
Pressure gauge	XCQ-062 (Kulite Semiconductor Products Inc.)
Data logger	EDX-3000 (Kyowa Electronic Instruments Co., Ltd.)

Table 2 presents the specifications of the wind tunnel models. Figure 2 illustrates the model shapes considered in this study. These moments of inertia include the rotational fixture. All capsules have a diameter of 80mm. As shown in Figure 2-(d), the pressure was measured at a radial distance of 20mm and at an axial distance of 80mm from the front edge. The experimental evaluation includes two aspects: the influence of the moment of inertia and the impact of capsule shape. Regarding the effect of moment of inertia, two scenarios were examined for the reference model (Al): one with a moment of inertia approximately half of the original value, and another with a moment of inertia four times the original value. As for the shape effect, two alternative models were utilized in comparison to the reference model (Al): the flat model, which featured a planar rear surface, and the ball model, which exhibited a more inflated shape. Figure 3 shows the photograph for the reference model (Al) and Ball model in TWT. As shown in Figure 3-(b), the shape prone to collision with the sting during free oscillation were removed. The rotational center for all capsules remained constant, situated at a distance of 13.3mm from the front end. This position corresponds to approximately 66.6% of the total length. The model was supported by a rear sting through bearings, allowing for oscillation within a range of up to approximately 60 degrees.

DOI: 10.13009/EUCASS2023-407

Table 2: Specifications of wind tunnel models

	Material	Moment of inertia for pitch direction, g mm^2
Reference model (Al)	Al	1.06×10^{4}
Reference model (EPX82)	EPX82	0.49×10^{4}
Reference model (Brass)	Brass	4.05×10^{4}
Flat model	Al	2.08×10^{4}
Ball model	Al	4.16×10^{4}

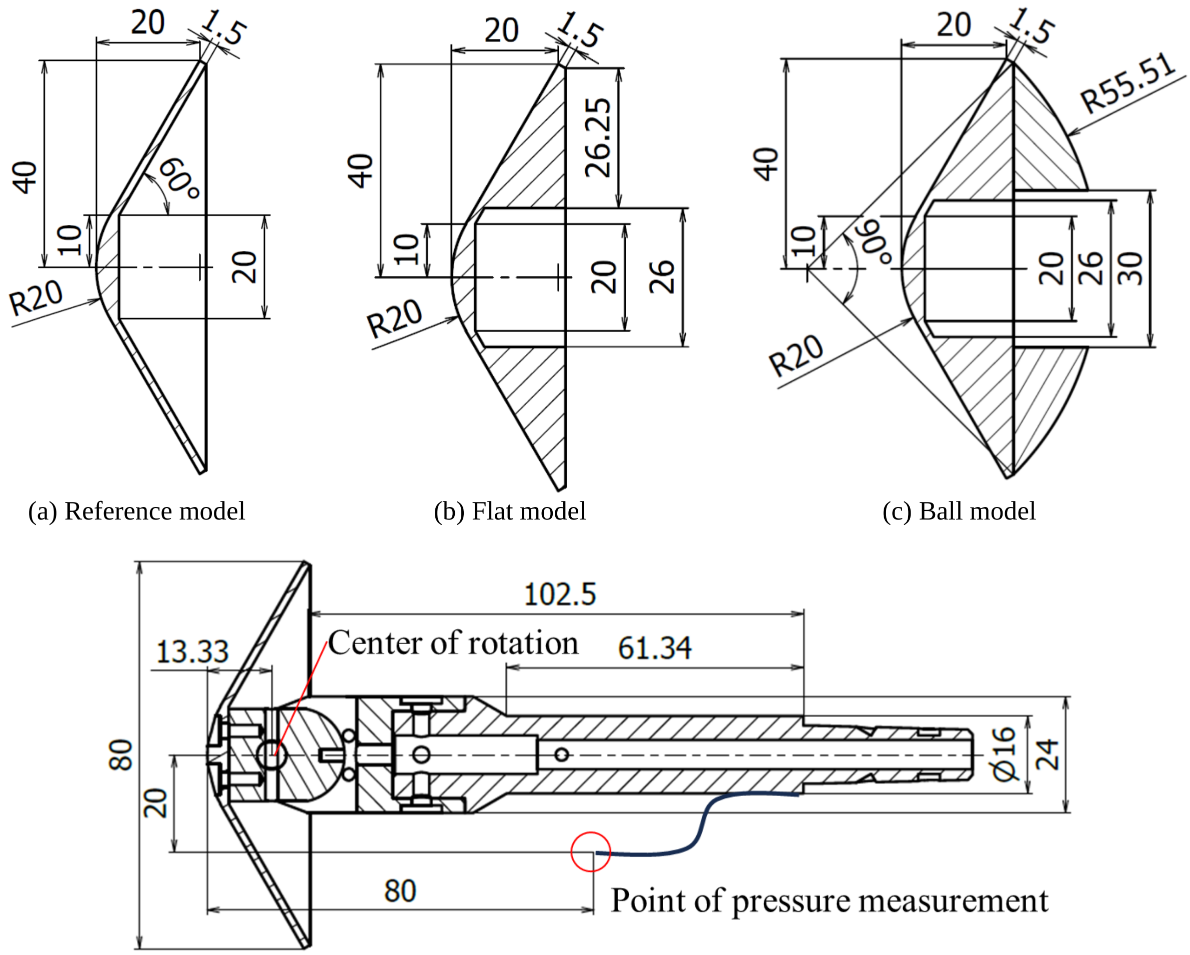

(a) Reference model (b) Flat model (c) Ball model

(d) Reference model with sting

Figure 2: Shape of model

DOI: 10.13009/EUCASS2023-407

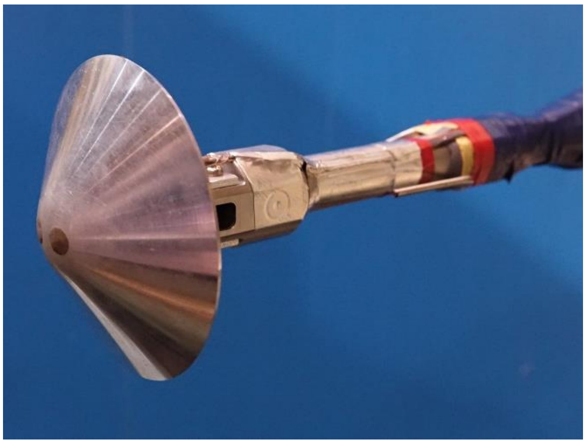
(a) Reference model (Al)

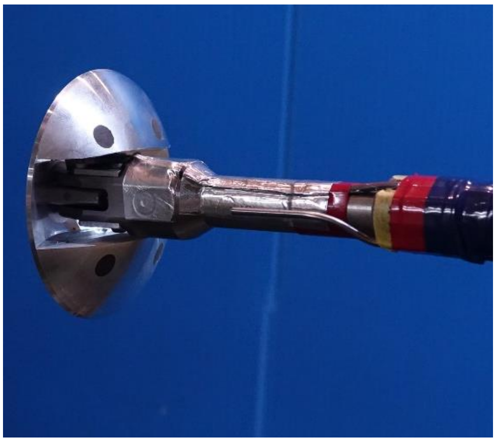
(b) Ball model

Figure 3: Photograph in TWT

Table 3 lists the experimental conditions. The diameter of capsule was used as a representative length for the Reynolds number. The capsule was initially set at a zero-degree AOA, and after stabilization of wind, the lock was released, initiating a uniaxial free motion. Data acquisition was conducted for a duration of at least 10 seconds. The trim angle of this capsule is 0 degrees.

Table 3: Experimental conditions

Mach number	1.3
Reynolds number	1.9e6
Velocity, m/s	386.6
Temperature of uniform flow, K	219.9
Density of uniform flow, kg/m^3	0.882
Diameter, m	0.08
Sampling rate of data, kHz	10
Initial AOA, deg.	0

3. Results and discussion

The instantaneous Schlieren images for the reference model (Al) are shown in Figure 4. Due to the lateral cut, the white region represents the expansion on the upper of the figure, while the black region represents the compression. On the lower surface, the white region indicates compression, and the black region represents expansion. The image corresponds to the lateral oscillation of the capsule. As the freestream Mach number exceeds 1, a shock wave was observed at the front of the capsule. The interaction between this shock wave and the wind tunnel wall can also be observed. The flow detaches from the shoulder region and flows downstream while expanding.

DOI: 10.13009/EUCASS2023-407

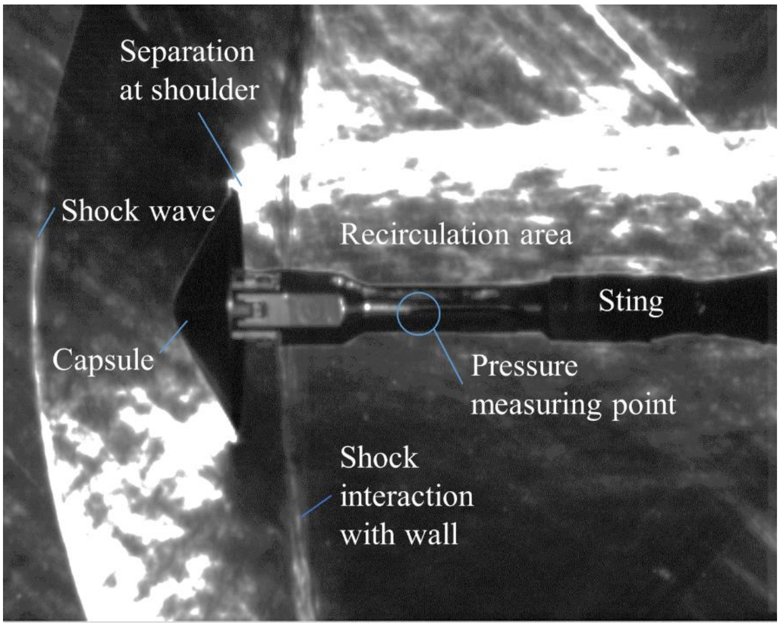

Figure 4: Instantaneous Schlieren images for the reference model (Al)

The histories of AOA for each model are shown in Figure 5. The FFT analysis results for the AOA and pressure histories are shown in Figure 6 for the reference model (Al). Table 4 presents the experimental results for each model. The mean amplitude of AOA was calculated by averaging the AOA between 5-10 seconds. As shown in Figure 5, once the capsule is released and enters a state of free oscillation, it quickly settles into a limit cycle where the amplitude of AOA becomes constant. As the moment of inertia increases, the oscillations become slower, and the time that it takes for the limit cycle to reach becomes longer. From the FFT analysis results, it can be inferred that capsules with higher moments of inertia exhibit higher intensity and dominance at the peak frequency. The lower amplitude for capsules with lower moments of inertia suggests that they were more stable, potentially suppressing motion and resulting in a lower intensity at the peak. Furthermore, the FFT results for the pressure history in the wake reveal two peaks, with one corresponding to the motion of oscillation and the other occurring at twice that period, which was associated with oscillations in the drag direction.

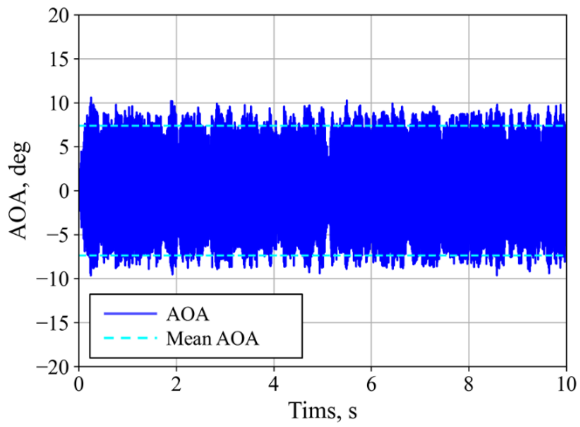

(a) Reference model (Al)

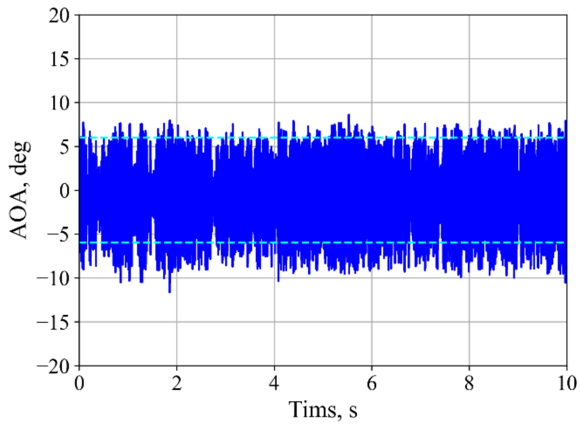

(b) Reference model (EPX82)

DOI: 10.13009/EUCASS2023-407

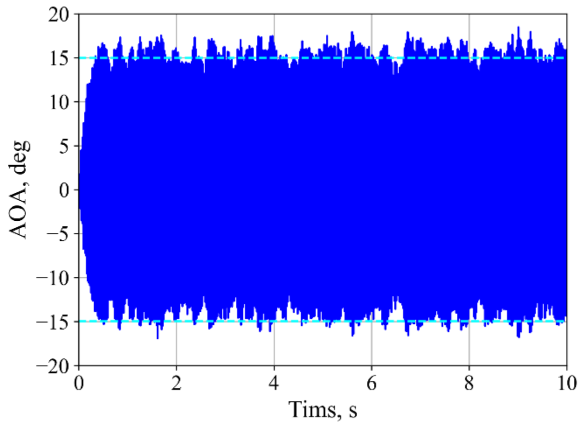

(c) Reference model (Brass)

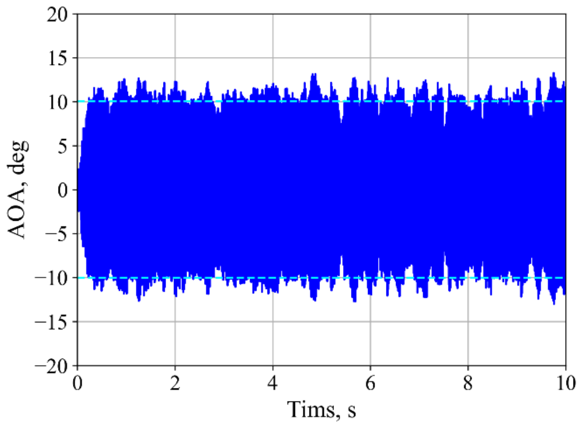

(d) Flat model

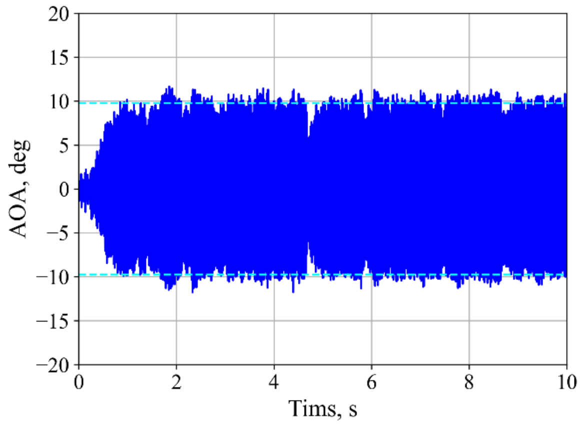

(e) Ball model

Figure 5: Time history of AOA for each model

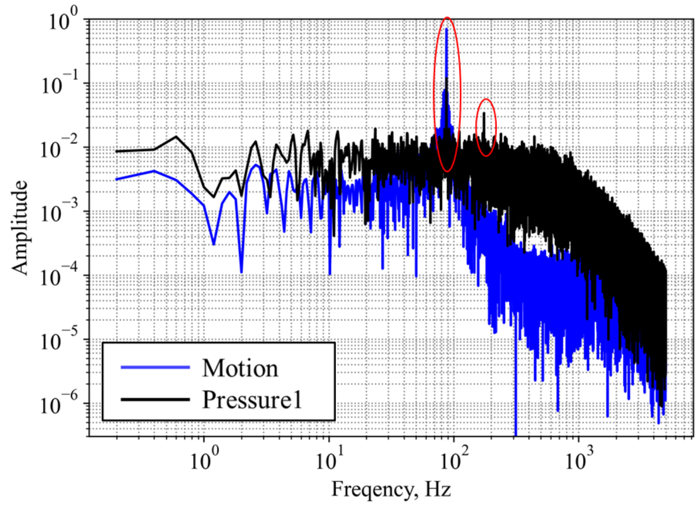

Figure 6: FFT analysis results of motion and wake pressure for reference model (Al)

DOI: 10.13009/EUCASS2023-407

Table 4: Summary of results measured in wind tunnel tests

	Mean amplitude of AOA, deg	Peak frequency of AOA, Hz	Amplitude at peak frequency for AOA	Peak frequency of Pressure, Hz
Reference model (Al)	7.4	87.6	0.70	87.6
Reference model (EPX82)	5.9	118.4	0.27	118.4
Reference model (Brass)	15.0	49.0	0.79	49.0
Flat model	10.0	68.2	0.65	68.2
Ball model	9.8	49.4	0.82	49.4

The FFT analysis results confirm that the motion frequency decreases as the moment of inertia increases. The motion equation for instability is described as equation (1), where I represent the moment of inertia, θ denotes the AOA, ρ is the density, u is the velocity, S represents the projected area, D is the reference length, Cmq is the damping coefficients, and Cma is the slope of static moment around 0 degrees. Considering only the static characteristics based on previous studies [8], the motion period can be expressed as equation (2), where *f* represents the frequency. In the case of the present capsule, which does not have a trim angle, the static pitching moment slope primarily depends on the front face of the capsule. Therefore, even when the rear surface of the capsule was modified, the static pitching moment slope was unlikely to change significantly. Figure 7 shows the profiles of the dimensionless frequency and dimensionless moment of inertia derived from equation (2). Hence, it could be inferred that for capsules with the same shape but different rear surfaces, the motion frequency would vary in proportion to the moment of inertia, following a similar slope.

$$I^* \frac{d^2\theta}{dt^2} = C_{mq}\frac{D}{u}\frac{d\theta}{dt} + C_{ma}\theta$$
$$I^* = \frac{I}{\frac{1}{2}\rho u^2 SD} \tag{1}$$

$$f \propto \left(-\frac{C_{m\alpha}}{I^*}\right)^{0.5} \tag{2}$$

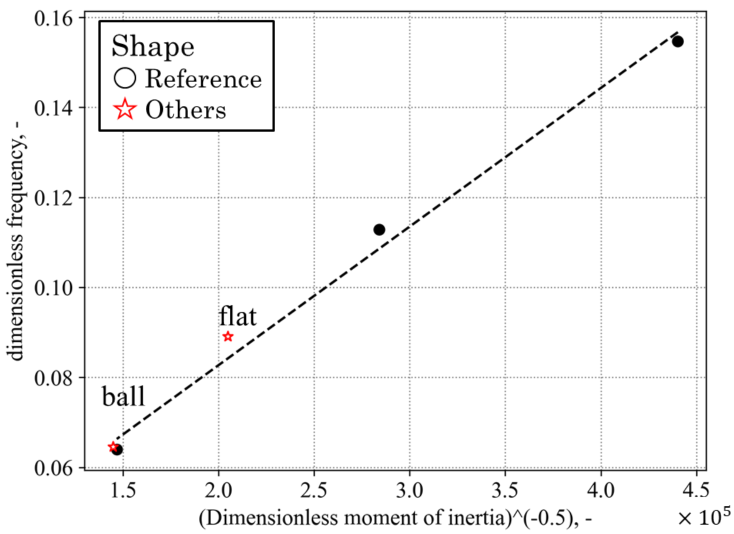

Figure 7: Dimensionless frequency and dimensionless moment of inertia derived from Equation (2)

Figure 8 shows the relation between the dimensionless moment of inertia and the amplitude of AOA. The maximum amplitude of AOA observed among all the data points after the start of motion was considered as the Max AOA. In the reference models, increasing the moment of inertia leaded to an increase in the mean amplitude of AOA. In the ball

DOI: 10.13009/EUCASS2023-407

model, which features a modified rear surface, the moment of inertia was similar to that of the reference model (Brass), but the mean amplitude of AOA was low. One possible factor contributing to this was the phase delay of pressure. The phase delay of pressure refers to the delayed arrival of the flow, returning from the wake to the rear surface of the capsule, compared to the motion cycle, which promotes the motion. Although the capsules have the same motion cycle due to similar moment of inertia, the inflation of the rear surface alters the delay of pressure pushing against the rear surface of the capsule, leading to a more stable transition. Conversely, it is possible that inflating the rear surface could result in instability in a different velocity range. For a more detailed understanding of the phenomena, it would be necessary to conduct a coupled analysis of fluid-motion interaction.

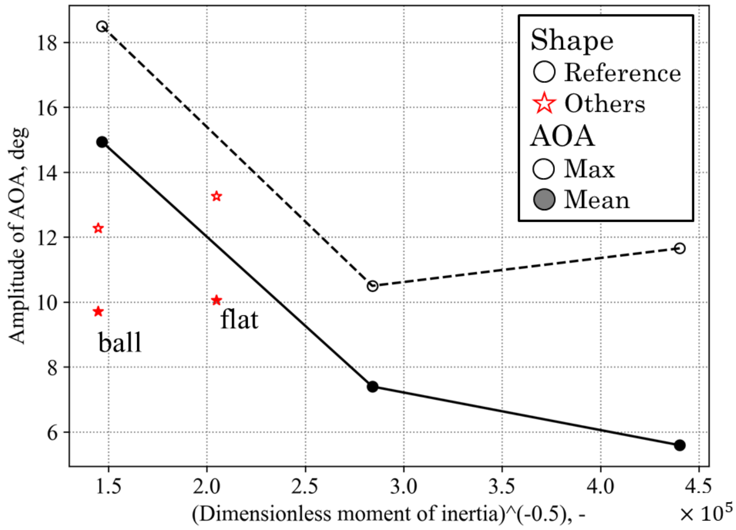

Figure 8: AOA against dimensionless moment of inertia

To evaluate the region of instability in the motion history, the damping coefficient is derived from Equation (1) by transforming it into Equation (3). The constant Cma was obtained from previous studies [3] as -0.023 rad^{-1}, assuming a low oscillation range. Since the AOA was measured in this experiment, the angular velocity and angular acceleration were calculated by differentiating the AOA with respect to time. Prior to differentiation, a Fourier expansion fitting was performed [9]. The fitted function obtained from this fitting was then differentiated to obtain the angular velocity and angular acceleration. For each history, the data was divided into segments of 4 cycles and fitted using a Fourier expansion up to n=24. The resulting damping coefficient is shown in Figure 9. The right-hand side of Equation (3) was divided by the angular velocity. Therefore, as the amplitude reaches its maximum at zero angular velocity, the value diverges. In the case of the reference (Brass) and Ball model cases, the dynamic stability coefficient was positive at zero AOA. This suggests that these two cases were more unstable and prone to oscillation at lower AOAs. Furthermore, comparing the reference (Brass) and Ball model cases, the Ball model case exhibits stronger stabilizing effects and lower amplitudes as the AOA increases, in contrast to the reference (Brass) case. On the other hand, the reference (Al) and reference (EPX82) cases did not indicate a significant positive value at zero AOA. This indicates a higher level of stability for others.

$$C_{mq} = \frac{u}{D\frac{d\theta}{dt}}\left(I^* \frac{d^2\theta}{dt^2} - C_{ma}\theta\right) \tag{3}$$

$$\begin{aligned} \theta &= \Sigma_{\mathrm{m}=1}^{n}(a_m \cos\omega_0 t + b_m \sin\omega_0 t) \\ a_m &= \frac{2}{T_0}\int_{-\frac{T_0}{2}}^{\frac{T_0}{2}} \theta \cos m\omega_0 t \; dt \\ b_m &= \frac{2}{T_0}\int_{-T_0/2}^{T_0/2} \theta \sin m\omega_0 t \; dt \end{aligned} \tag{4}$$

DOI: 10.13009/EUCASS2023-407

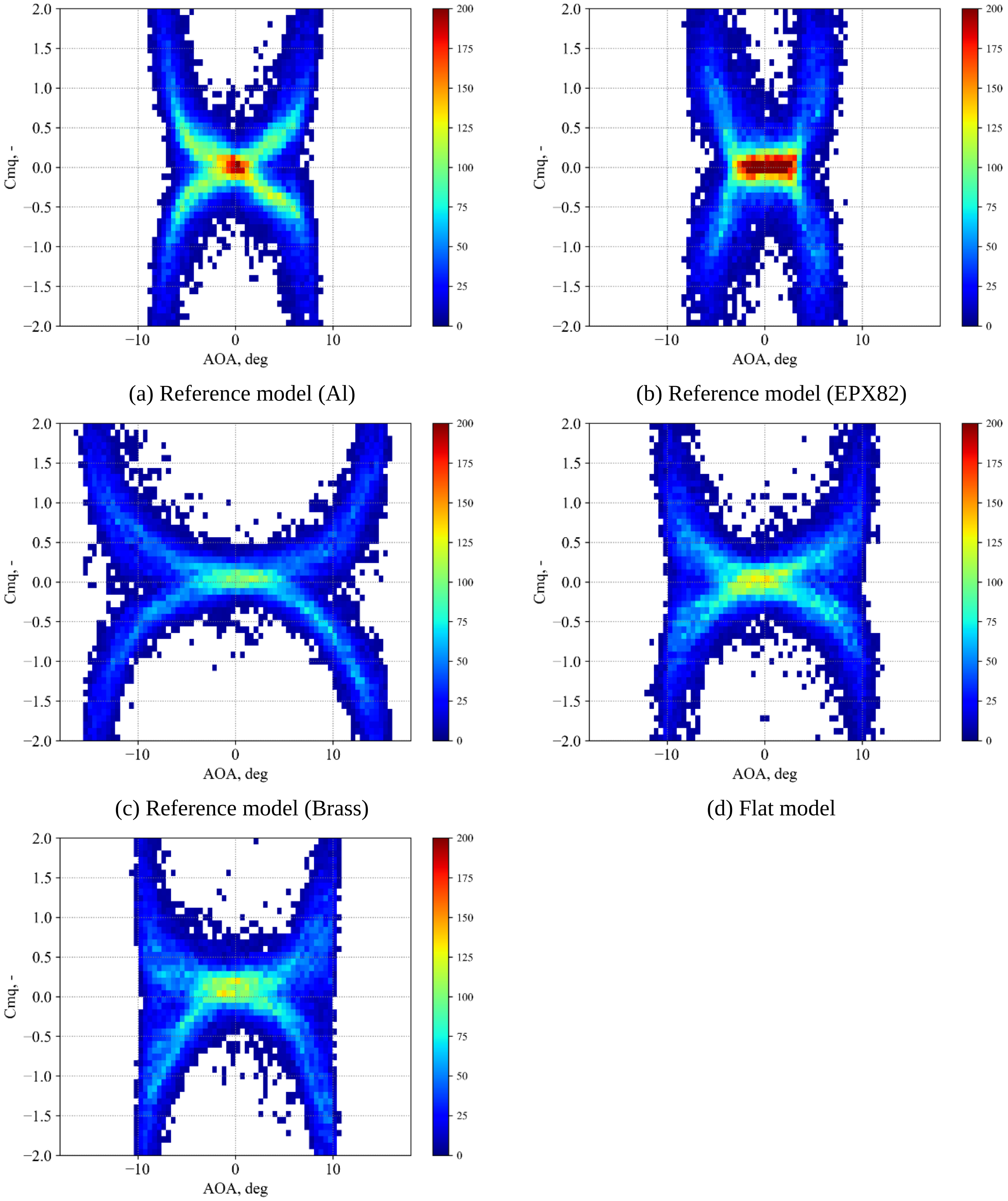

(a) Reference model (Al)

(b) Reference model (EPX82)

(c) Reference model (Brass)

(d) Flat model

(e) Ball model

Figure 9: Damping coefficient against AOA from Equation (3)

4. Conclusion

To evaluate the dynamic instability of thin-shell aeroshell-type capsules in the transonic regime, one-axis free oscillation tests in the pitch direction were conducted using a transonic wind tunnel. As an exploration of instability

DOI: 10.13009/EUCASS2023-407

mitigation methods, the same tests were conducted using capsules with varied moments of inertia and capsules with an inflated rear surface.

It was observed that increasing the moment of inertia in the reference shape resulted in a larger amplitude of AOA. However, even with similar moment of inertia, the Ball model with an inflated rear surface exhibited relatively lower amplitudes. Comparing the damping coefficients calculated using Fourier transform-based fitting, it was suggested that the Ball model with an inflated rear surface exerted stronger stabilizing forces as the AOA increased. Furthermore, the frequency relation derived from the equations of motion for instability could be reproduced, and since the slope of static moment is predominantly determined by the frontal shape, capsules with different rear shapes could be predicted to move along the same straight line. In the wake region, it was demonstrated that the oscillation period of the capsule and the double period in the drag direction dominated. Therefore, it is suggested that inflating the rear surface of the thin aeroshell capsule contributes to stability in the transonic regime.

Obtaining detailed flow field data from experimental measurements is challenging, and there are still many unclear factors in this phenomenon. Therefore, in the future, it is necessary to reproduce the free oscillation test using fluid-motion interaction simulation and approach this phenomenon from the perspective of the flow field.

Acknowledgment

This study was supported by JSPS KAKENHI (Grant No.20H02360) and JST SPRING (Grant Number JPMJSP2119). The wind tunnel experiments were conducted at a transonic wind tunnel provided by the Japan Aerospace Exploration Agency as an inter-university research institute facility (Project ID: W20-001).

References

[1] Kazuhiko, Y., Toshiyuki, S., Hiroki, T., Takashi, O., Aoi, H., and Tomonari, O., 2020. Proposal for Advanced Sample Return Capsule for Deep Space Exploration with Small Spacecraft. In: *Proceedings of 64th Space Sciences and Technology Conference*, JSASS-2020-4626-4F02.

[2] Yamada, T., and Yoshihara, K., 2022. Post-Flight Analysis of Recovered Components of Hayabusa2 Sample Return Capsule. In: *proceedings of 33rd Int. Symp. Space Technology and Science (33rd ISTS)*.

[3] Takasawa, H., Fujii, T., Takahashi, Y., Nagata, Y., Yamada, K., and Takayanagi, H., 2022. Experimental and Numerical Study on Aerodynamic Instability of Thin Shell Type Reentry Capsule at Subsonic Speed. In: *proceedings of 33rd Int. Symp. Space Technology and Science (33rd ISTS)*.

[4] Takasawa, H., Suenaga, Y., Miyashita, T., Hirata, K., Wakabayashi, K., Takahashi, Y., Nagata, Y., and Yamada, K., 2023. Flight Demonstration for Reentry Capsule with Thin Aeroshell Using Rubber Balloon. In : *proceedings of 34rd Int. Symp. Space Technology and Science (34rd ISTS)*.

[5] Teramoto, S., Hiraki, K., and Fujii, K., 2001. Numerical analysis of dynamic stability of a reentry capsule at transonic speeds. *AIAA Journal*. 39:646–653. https://doi.org/10.2514/2.1357.

[6] Baillion, M., 1997. BLUNT BODIES DYNAMIC DERIVATIVES. NATO Advisory Group for Aerospace Research and Development Rept. AGARD-R-808.

[7] Yoshinaga, T., Tate, A., Watanabe, M., and Shimoda, T., 1996. Orbital re-entry experiment vehicle ground and flight dynamic test results comparison. *Journal of Spacecraft and Rockets*, 33(5) :635-642, https://doi.org/10.2514/3.26813.

[8] Schoenenberger, M., Norman, J.V., Karlgaard, C., Kutty, P., and Way, D., 2014. Assessment of the reconstructed aerodynamics of the Mars science laboratory entry vehicle. *Journal of Spacecraft and Rockets*, 51(4) :1076-1093. https://doi.org/10.2514/1.A32794.

[9] Koga, S., Hidaka, A., Tagai, R., Kimura, T., Yoshinaga, T., Nagai, S., and Nishijima, H., 2010. Dynamic stability testing of a reentry lifting capsule in a transonic wind tunnel. In : *52nd Aerospace Sciences Meeting*, p.1119. https://doi.org/10.2514/6.2014-1119.